AUTOMATIC DETECTION AND 2D AREA ESTIMATION OF BRAIN TUMORS FROM MRI USING DEEP LEARNING APPROACHES

TỰ ĐỘNG PHÁT HIỆN VÀ ƯỚC LƯỢNG DIỆN TÍCH 2D CỦA KHỐI U NÃO TỪ ẢNH MRI BẰNG CÁC PHƯƠNG PHÁP HỌC SÂU

Hoang-Dung Nguyen*, Hoang-Dang Le, Thi Tra My Do

Faculty of Automation Engineering, Can Tho University, Can Tho city, Vietnam

*Corresponding author: hoangdung@ctu.edu.vn

(Received: January 01, 2026; Revised: March 20, 2026; Accepted: April 14, 2026)

DOI: 10.31130/ud-jst.2026.24(5A).003E

Abstract - This study proposes an automated method for detecting and assessing brain tumors from magnetic resonance imaging (MRI) using a deep learning model, ResU-Net. The MRI data, sourced from the low-grade glioma (LGG) Segmentation dataset on Kaggle, consist of images from patients diagnosed with low-grade gliomas. After pre-processing, the data were split into training, validation, and testing sets. The ResU-Net model was trained to segment and detect the presence of brain tumors. Additionally, the tumor region area was calculated to support the evaluation of the disease. The performance of ResU-Net was compared with other deep learning architectures including U-Net, FC-DenseNet, and DeepLabV3+. The experimental results show that both ResU-Net and DeepLabV3+ achieved the highest detection accuracy of 96% on the test dataset. However, in terms of the segmentation performance, ResU-Net obtained the highest Dice score of 92%, indicating predicted tumor regions closing to the ground truth.

Key words - Automatic tumor detection; brain tumor; deep learning; magnetic resonance imaging (MRI); ResU-Net

Tóm tắt - Nghiên cứu này đề xuất một phương pháp tự động phát hiện và đánh giá khối u não từ ảnh cộng hưởng từ (MRI) bằng cách sử dụng mô hình học sâu ResU-Net. Dữ liệu MRI, được lấy từ bộ dữ liệu LGG Segmentation trên Kaggle, bao gồm hình ảnh của các bệnh nhân được chẩn đoán mắc u thần kinh đệm độ thấp. Sau bước tiền xử lý, dữ liệu được chia thành các tập huấn luyện, xác thực và kiểm thử. Mô hình ResU-Net được huấn luyện để phân đoạn và phát hiện sự hiện diện của khối u não. Ngoài ra, diện tích vùng khối u cũng được tính toán nhằm hỗ trợ đánh giá mức độ của bệnh. Hiệu suất của ResU-Net được so sánh với các kiến trúc khác như U-Net, FC-DenseNet và DeepLabV3+. Kết quả thực nghiệm cho thấy, ResU-Net và DeepLabV3+ đạt độ chính xác phát hiện khối u cao nhất là 96% trên tập kiểm tra. Tuy nhiên, đối với hiệu suất phân đoạn, ResU-Net đạt Dice score cao nhất là 92%, cho thấy mức độ trùng khớp của bướu não được ước lượng với bướu não thực tế.

Từ khóa - Phát hiện khối u tự động; khối u não; học sâu; ảnh cộng hưởng từ (MRI); ResU-Net

1. Introduction

Brain tumors result from the abnormal and uncontrolled growth of cells within the brain [1-3]. They are generally classified into two categories: benign and malignant. Both types can pose serious health risks, with malignant tumors typically exhibiting rapid growth and the potential to invade or metastasize to other parts of the body. Brain tumors are commonly diagnosed through imaging techniques such as computed tomography (CT), magnetic resonance imaging (MRI), and positron emission tomography (PET), or via clinical tests including biopsy and cerebrospinal fluid analysis [4-7]. Early detection plays a critical role in improving treatment outcomes and increasing the survival rate of patients.

In recent years, artificial intelligence (AI), particularly deep learning (DL) techniques, has experienced rapid advancements and opened up a wide range of applications across various domains, especially in healthcare [8-10]. In the field of medical imaging, deep learning architectures such as GoogLeNet, U-Net, VGG, ResNet, Inception, DenseNet, and DeepLab have been widely adopted for brain tumor detection and classification tasks [11-14]. One of the most prominent applications is the identification and classification of brain tumors from MRI images, which greatly assists physicians in making accurate diagnoses and formulating effective treatment plans [15, 16]. The integration of DL approaches into medical practice promises higher diagnostic accuracy, reduced processing time, and minimized subjectivity compared to traditional methods.

Among DL models, the U-Net is one of the most pioneering and widely adopted architectures for brain tumor segmentation in medical imaging [17]. Variants of U-Net, such as ResU-Net [18], FC-DenseNet [19], and DeepLabV3+ [20], have been developed to further enhance feature extraction capabilities and improve segmentation accuracy. However, the performance of each model varies depending on the dataset characteristics and training conditions.

U-Net follows a symmetric encoder–decoder architecture, connected through a central bottleneck. The encoder is responsible for extracting hierarchical features via convolutional blocks (ConvBlock) and progressively reducing spatial resolution using max pooling layers [21]. Conversely, the decoder restores the original image resolution through upsampling layers (UpConv), while incorporating corresponding features from the encoder via skip connections. These skip connections help retain important spatial details that may be lost during downsampling. Typically, the input MRI image has a size of 256×256×3, and the output is a binary segmentation map of size 256×256×1 [22], representing the tumor region. It should be noted that although original MRI scans are

single-channel grayscale images, they are converted to a 3-channel RGB format to maintain consistency with common DL input standards and to facilitate potential integration with pre-trained models in future extensions.

ResU-Net is constructed based on a symmetric encoder–decoder architecture similar to U-Net, with the key distinction being the replacement of standard convolutional blocks by ResNet blocks [23]. The integration of internal residual connections enhances feature extraction capability and mitigates information loss during. The image resolution is progressively downsampled from 256×256 to 16×16, while the number of feature maps increases accordingly to capture deeper semantic representations.

On the other hand, FC-DenseNet leverages Dense Blocks to promote feature reuse [24, 25]. Its architecture also comprises three main components: encoder, bottleneck, and decoder. The encoder processes the input image of size 256×256×3 using a 3×3 convolution layer with 48 filters to extract initial features. The bottleneck section utilizes a specialized Dense Block with a higher number of filters to optimize deep feature learning before transitioning to the decoder [26, 27]. The decoder includes Transition Up layers (via upsampling or transposed convolution) to restore the image resolution, followed by Dense Blocks to recover detailed information.

DeepLabV3+ adopts an encoder–decoder architecture but introduces several notable enhancements compared to previous models [18, 28]. This architectural design can improve the model's ability to detect objects of varying sizes and shapes, such as brain tumors. For DL architectures of U-Net, ResU-Net, FC-DenseNet, and DeepLabV3+ promise results in medical image segmentation. ResU-Net gives an advantage for segmenting heterogeneous and small tumor regions by enhanced gradient flow and feature retention capabilities [29].

This work aims to detect and estimate the brain tumor with the low-grade glioma (LGG) using the ResU-Net DL model. The dataset consists of 2,856 2D slices derived from 110 patients available from Kaggle. The important indices are evaluated, such as accuracy, precision, dice score, and IoU. Finally, the proposed approach is compared with the U-Net, FC-DenseNet, and DeepLabV3+ to assess its performance.

2. Research methodology

The dataset utilized in this study is the LGG segmentation dataset with LGG cases available from Kaggle. It contains 3D MRI images of patients diagnosed with low-grade brain tumors. The data origin is detailed in the study conducted by the Cancer Genome Atlas Research Network. Both tumor and non-tumor images were split into training, testing, and validation sets in a (70:10:20) ratio, as illustrated in Figure 1. In this work, total of 2,856 2D slices derived from 110 patients were utilized. It should be noted that the data splitting was performed at the slice level rather than the patient level, meaning slices from the same patient may appear in different sets. This approach was taken due to dataset constraints, though patient-wise splitting would be preferable for clinical validation.

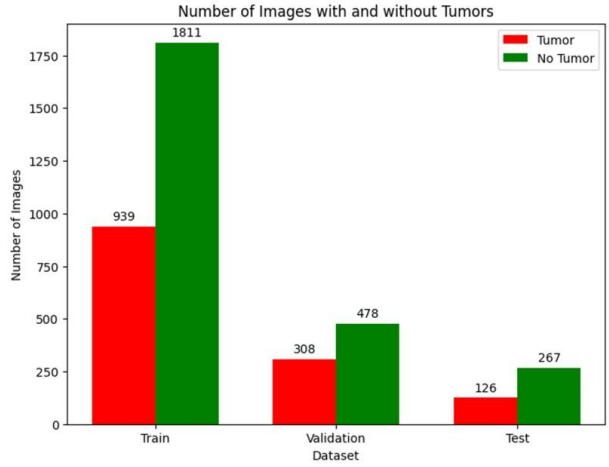

Figure 1. *The dataset is split into (Train:Test: Validation) in a (70:10:20) ratio*

In this study, Google Colab is utilized as the programming environment, integrated with GPU hardware to optimize the training process of deep learning models. The hardware setup includes an NVIDIA A100-SXM4-40GB GPU with 42.5 GB of VRAM, an Intel(R) Xeon(R) CPU running at 2.20GHz, 89.6 GB of RAM, and 50 GB of storage via Google Drive. The utilized main programming language is Python 3.10. The software stack includes TensorFlow 2.11, Keras, and PyTorch for deep learning, along with NumPy, Pandas, OpenCV, Matplotlib, and Seaborn for data processing and visualization.

2.1. Data pre-processing

Figure 2 illustrates an example of an original MRI scan (Figure 2(a)) and its corresponding mask (Figure 2(b)) from the LGG Segmentation Dataset. The 3D MRI volumes in the dataset are sliced into 2D images and resized to a standardized resolution of 256×256 pixels. The preprocessing steps include intensity normalization to balance the image contrast, scaling pixel values to the [0, 1] range, and converting labels into binary format to distinguish between tumor and non-tumor brain images.

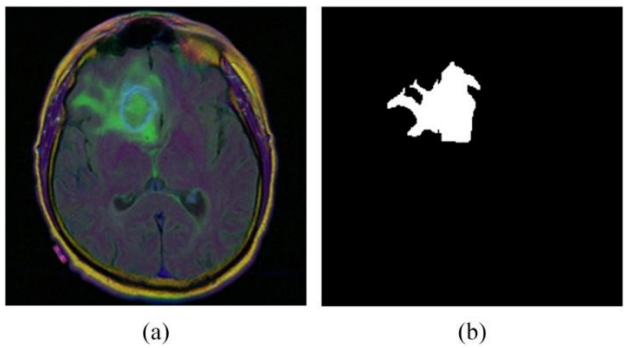

Figure 2. *Original MRI image (a) and its corresponding mask (b) from the LGG segmentation dataset*

In this study, the ResU-Net model is employed for brain tumor segmentation and its area estimation. Its performance is compared against three other models including U-Net, FC-DenseNet, and DeepLabV3+. All models are trained under the same conditions, including 200 training epochs, an initial learning rate of 0.001, the Adam optimizer, and the Dice Loss function as the evaluation metric.

2.2. ResU-Net DL architecture

ResU-Net is an enhanced variant of the U-Net architecture that incorporates residual blocks to improve gradient flow during deep network training. Figure 3 illustrates the overall structure of the ResU-Net model. Similar to U-Net, ResU-Net consists of two main components: an encoder and a decoder. In the encoder block, ResNetConv modules are employed to enhance feature extraction capabilities and mitigate information loss during backpropagation, thanks to internal residual connections [12, 13]. The spatial resolution of the feature maps is progressively reduced through the layers: from 256×256 → 128×128 → 64×64 → 32×32 → 16×16, while the number of feature channels increases.

The decoder block utilizes up-sampling layers to restore the original image resolution and integrates contextual information from the encoder via skip connections, which help to accurately recover fine image details. The final output of the ResU-Net model is a binary image of size 256×256×1, representing the segmented brain tumor region.

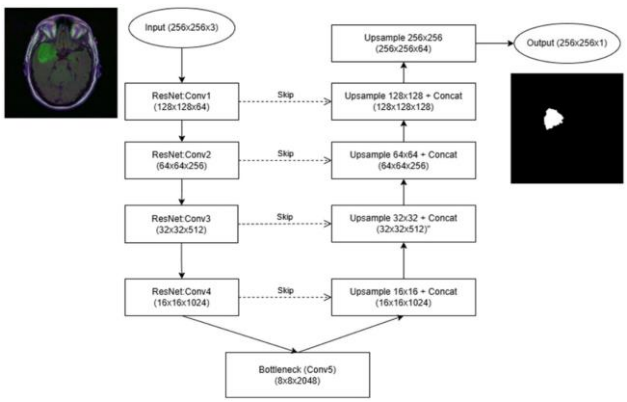

Figure 3. *Architecture of the ResU-Net model*

2.3. Model evaluation metrics

To evaluate the performance of the segmentation models, this study employs commonly used metrics, including Accuracy, Precision, Recall, F1-Score, IoU, and Dice Coefficient [30]. The formulas for these metrics are presented as follows.

Accuracy: The ratio of correctly classified pixels (both tumor and non-tumor regions) to the total number of pixels. However, accuracy can be misleading in the case of imbalanced data (e.g., the tumor region is much smaller than the background).

Precision (Positive Predictive Value): Indicates how many of the pixels predicted as tumor by the model are actually tumor pixels. High precision means the model generates fewer false positives.

Recall (Sensitivity): The proportion of ground truth tumor pixels correctly identified by the model. High recall ensures that tumor regions are not missed.

F1-Score: The harmonic mean of Precision and Recall, providing a balanced 2D area estimation between false positives and false negatives.

IoU (Intersection over Union): Measures the overlap between the predicted segmentation and the ground truth, calculated as the ratio of their intersection over their union. It is widely used in segmentation tasks.

Dice Coefficient: Similar to IoU but places more emphasis on the overlapping region. It is frequently used in medical image analysis due to its ability to accurately evaluate small lesion regions.

All these metrics are calculated on the test set and are utilized to objectively compare the performance of different models.

2.4. Tumor area estimation from 2D slices

To evaluate a brain tumor, one of the key metrics is its area. By comparing the tumor area in the current MRI scan with previous scans, specialists can assess the effectiveness of the treatment. For instance, if the tumor area remains unchanged, it suggests that the treatment is effectively halting tumor growth. Conversely, an increase in tumor size indicates disease progression and implies that the current treatment regimen may be ineffective and needs revision.

In this study, the tumor area is determined based on the number of pixels identified as tumor regions in the MRI image. To compute the tumor area, the resolution of the MRI image in DPI (Dots Per Inch) is considered. The total tumor area is then given by

$$S_T = N_p \times S_p \tag{1}$$

where, S_T is the tumor area (mm²), N_p is the number of pixels identified as tumor tissue by the DL model. For MRI images with a DPI of 96, the side length of one pixel is calculated for $1\,\text{pixel} = \frac{25.4\text{mm}}{96} \approx 0.265\text{mm}$. Thus, the area of a single pixel is $S_p = 0.265^2 \approx 0.07\text{mm}^2$.

3. Results and discussion

3.1. Training performance evaluation

During the training phase, two key metrics were used to preliminarily assess the performance of the models: Dice Coefficient and Loss. Figures 4 and 5 illustrate the evolution of the Dice Coefficient and Loss values, respectively, throughout the training and validation processes for the four segmentation models: U-Net, ResU-Net, FC-DenseNet, and DeepLabV3+.

In terms of the Dice Coefficient, U-Net and FC-DenseNet achieved faster convergence (within 10 epochs) compared to ResU-Net and DeepLabV3+. Although ResU-Net required a longer convergence time, it achieved the highest segmentation accuracy of approximately 90% (see Figure 4b), while U-Net and FC-DenseNet both reached around 85% accuracy (Figure 4a and 4c). Among all models, DeepLabV3+ demonstrated the weakest performance, with slower convergence (around 25 epochs) and the lowest accuracy (approximately 70%) as shown in Figure 4d. Regarding the Loss metric, ResU-Net again showed superior performance, with the loss value approaching zero (Figure 5b). In contrast, the other three models maintained higher loss values around 0.2 (Figure 5a, 5c, and 5d).

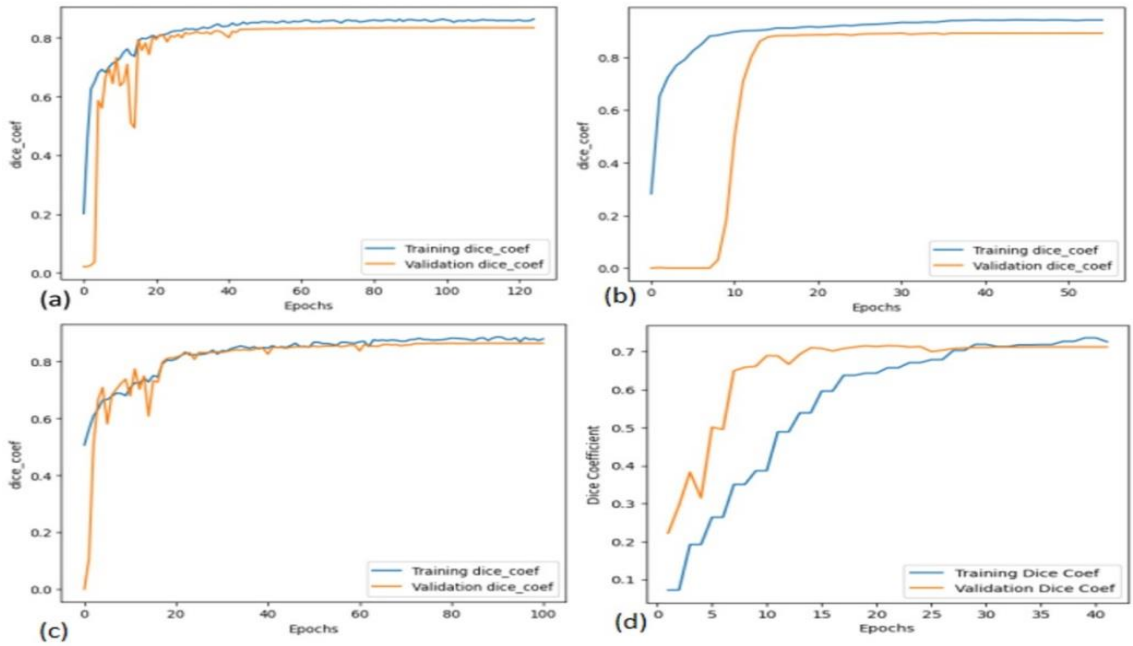

Figure 4. *Dice Coefficient plots for (a) U-Net, (b) ResU-Net, (c) FC-DenseNet, and (d) DeepLabV3+*

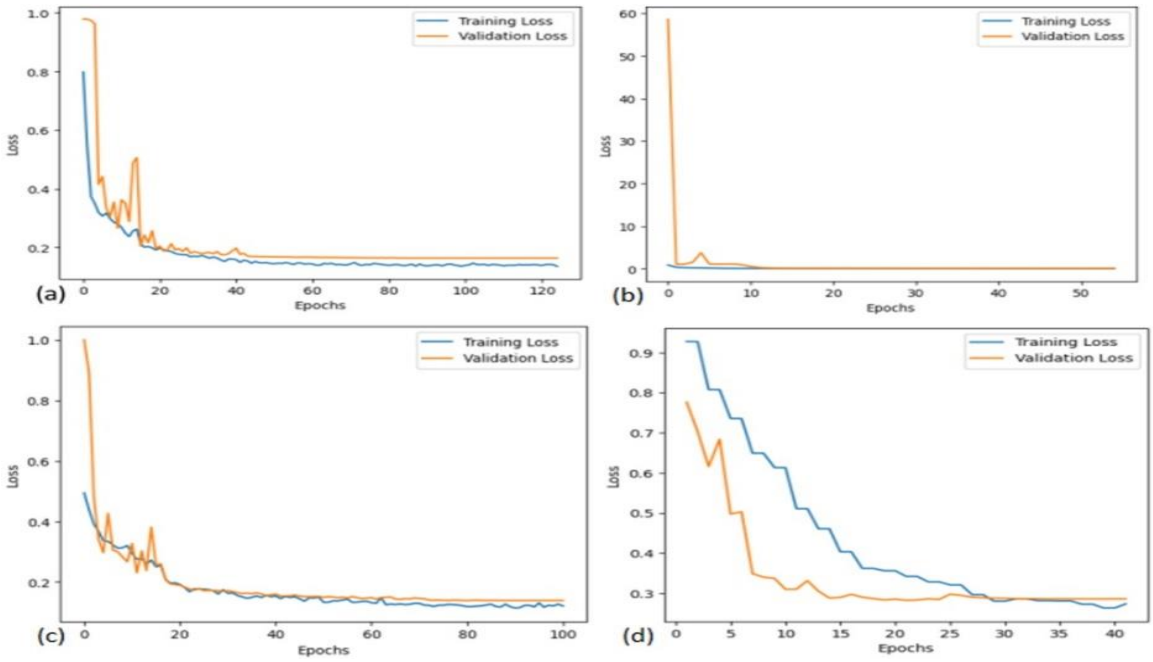

Figure 5. *Loss plots for (a) U-Net, (b) ResU-Net, (c) FC-DenseNet, and (d) DeepLabV3+*

Table 1. *Dice Coefficient and IoU Scores of Different Models on Train, Validation, and Test Sets (with 95% Confidence Intervals)*

Model	DICE-COEF			IoU		
	Train	Val	Test	Train	Val	Test
U-Net	0.89	0.85	0.85	0.86	0.82	0.82
ResU-Net	0.96	0.90	**0.92**	0.94	0.87	0.90
FC-DenseNet	0.92	0.87	0.89	0.89	0.83	0.87
DeepLabV3+	0.89	0.85	0.88	0.84	0.80	0.85

Note: *Values in brackets represent 95% confidence intervals for test set scores, calculated using bootstrapping with 1000 resamples.*

Table 1 presents a comparative analysis of Dice Coefficient and Intersection over Union (IoU) metrics for four deep learning models: U-Net, ResU-Net, FC-DenseNet, and DeepLabV3+, across training, validation, and testing datasets. Among these models, ResU-Net demonstrates better performance across all three data splits. It achieves the highest Dice scores of 96% (Train), 90% (Validation), and 92% (Test) with a 95% confidence interval of [0.91, 0.93], and corresponding IoU scores of 94%, 87%, and 90% with a confidence interval of [0.88, 0.92]. The non-overlapping confidence intervals between ResU-Net and U-Net indicate statistically significant superiority of ResU-Net on the test set. These results indicate that ResU-Net not only learns effectively from the training data but also generalizes well to unseen data.

FC-DenseNet also performs competitively, achieving Dice scores of 92%, 87%, and 89%, and IoU scores of 89%, 83%, and 87% for the same respective datasets. It is slightly lower than ResU-Net. However, FC-DenseNet is better than both U-Net and DeepLabV3+. DeepLabV3+ shows relatively moderate performance with Dice scores of 89%, 85%, and 88% for train, validation, and test, respectively and IoU scores of 84%, 80%, and 85%. In summary, ResU-Net achieves the best balance between learning capacity and generalization, making it the most effective model for brain tumor segmentation in this study.

3.2. Binary detection performance evaluation

Figure 6 illustrates the confusion matrices for four models (U-Net, ResU-Net, FC-DenseNet, and DeepLabV3+) in binary detection of tumor presence in brain MRI images into two categories: "Tumor" and "No Tumor". Each matrix presents the number of correctly and incorrectly classified MRI images. The U-Net model correctly classified 247 non-tumor images and 110 tumor images, but misclassified 20 non-tumor images as tumors and 16 tumor images as non-tumor (see Figure 6(a)), respectively.

The ResU-Net model achieved better performance, correctly identifying 260 non-tumor and 118 tumor images with only 7 non-tumor and 8 tumor images misclassified (see Figure 6(b)), respectively. FC-DenseNet correctly classified 253 non-tumor and 115 tumor images while misclassifying 14 non-tumor and 11 tumor images (see Figure 6(c)), respectively. Finally, DeepLabV3+ correctly detected 266 non-tumor and 112 tumor images while it misclassified 1 non-tumor and 14 tumor images (see Figure 6(d)), respectively.

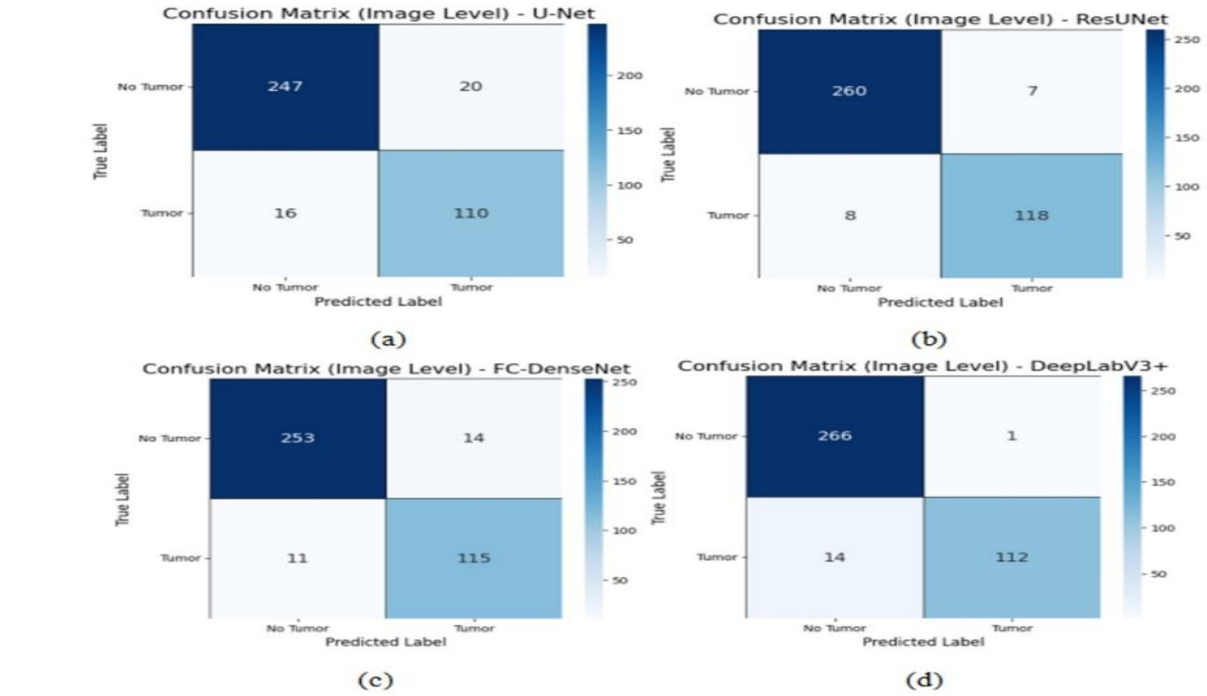

Figure 6. *Confusion matrices of the models: (a) U-Net model; (b) resU-Net model; (c) FC-DenseNet model; (d) DeepLabV3+ model*

Table 2. *Binary detection performance metrics*

Model	Accuracy	Precision	Recall	F1-Score
U-Net	0.91	0.85	0.87	0.86
ResU-Net	**0.96**	**0.94**	**0.94**	**0.94**
FC-DenseNet	0.94	0.89	0.91	0.90
DeepLabV3+	**0.96**	**0.99**	**0.89**	**0.94**

ResU-Net and DeepLabV3+ achieved the joint-highest overall accuracy (0.96) on the test set. However, it still misclassified 14 tumor images (see Figure 6(d)). Based on the confusion matrices, we calculated Precision, Recall, F1-Score, and Accuracy for each model (Table 2). McNemar's test was performed to compare the detection performance pairwise. The test indicated that the performance difference between ResU-Net and DeepLabV3+ was not statistically significant ($p > 0.05$). In short, ResU-Net demonstrated a balanced performance across both classes whereas DeepLabV3+ excelled in detecting non-tumor images but was slightly less accurate in identifying tumor cases. These results suggest that selecting the appropriate model depends on the dataset characteristics and application priorities, whether maximizing tumor detection or minimizing false alarms.

Similarly, the pairwise test of U-Net and ResU-Net U-Net ($\chi^2 = 8.64$, $p = 0.003$) indicated that ResU-Net is better performance than U-Net. However, there was no statistically significant difference between ResU-Net and DeepLabV3+ ($\chi^2 = 0.25$, $p = 0.617$).

3.3. Segmentation and tumor area estimation

Figure 7 shows the prediction results for two brain MRI images without tumors (Figure 7(a)), using four deep learning models: U-Net (Figure 7(c)), ResU-Net (Figure 7(d)), FC-DenseNet (Figure 7(e)), and DeepLabV3+ (Figure 7(f)). The experimental results indicate that all four models achieved 100% accuracy in correctly identifying tumor-free MRI scans.

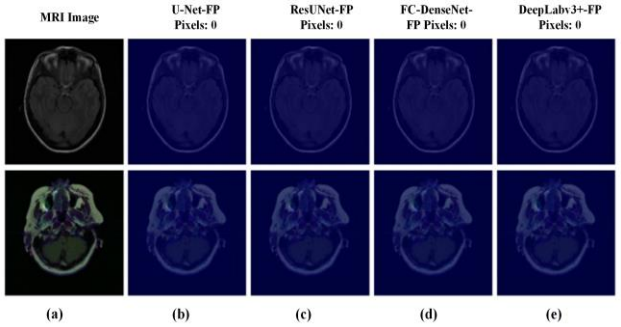

Figure 7. *MRI images without brain tumors: (a) original MRI images; (b) ground truth masks; (c) predicted masks by U-Net; (d) by ResU-Net; (e) by FC-DenseNet; (f) by DeepLabV3+*

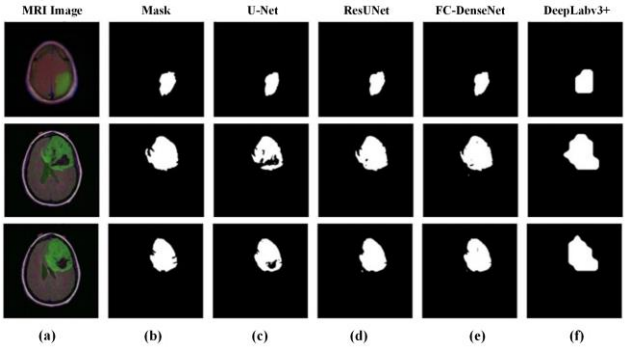

Figure 8. *MRI images with brain tumors: (a) original MRI images; (b) ground truth masks; (c) predicted masks by U-Net; (d) by ResU-Net; (e) by FC-DenseNet; (f) by DeepLabV3+*

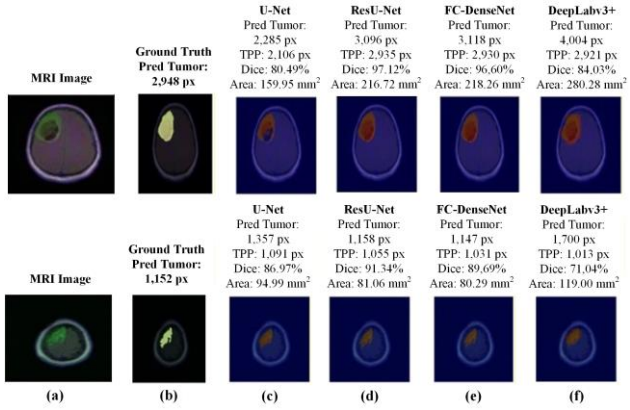

Figure 9. *Tumor region estimation based on pixel count: (a) original MRI image; (b) ground truth mask; (c) predicted mask from U-Net; (d) predicted mask from ResU-Net; (e) predicted mask from FC-DenseNet; (f) predicted mask from DeepLabv3. Embedded text boxes show the Dice (%) and Area (mm²) for each model prediction*

Figure 8 showcases the segmentation results of brain tumors from three different MRI scans using four DL models. For each case, the figure displays the original MRI image, the ground truth mask, and the predicted masks from U-Net, ResU-Net, FC-DenseNet, and DeepLabV3+. The findings reveal that while all models can detect tumor regions, their accuracy and consistency vary: (1) ResU-Net and FC-DenseNet exhibit the closest agreement with the ground truth, particularly for tumors with regular, simple shapes; (2) U-Net sometimes produces incomplete or irregular segmentations, especially along tumor boundaries; and (3) DeepLabV3+ delivers well-defined boundaries for large tumors but tends to blur or overestimate boundaries in cases of small or irregularly shaped tumors.

Figure 9 presents tumor segmentation results on two MRI images, along with key quantitative metrics including ground truth tumor pixels: the number of pixels representing the tumor region in the ground truth mask; predicted tumor pixels: the number of tumor pixels predicted by the DL models; Correctly predicted tumor pixels (TPP): the number of correctly identified tumor pixels; Dice (%): the Dice coefficient indicating the overlap between predicted and ground truth tumor regions; and Area is the estimated tumor area in mm² computed from Eq. (1). And the comparison focuses on ground truth tumor pixels versus predicted values, with the absolute area difference (mm²) utilized as the key metric for accuracy evaluation.

Table 3. *Comparison of tumor area estimation capabilities among DL models*

MRI images with a tumor	Ground Truth & Predicted tumor	Models			
		U-Net	ResU-Net	FC-DenseNet	DeepLabV3+
Figure 9 (upper panel)	Ground truth tumor (Pixels)	2,948	2,948	2,948	2,948
	Predicted tumor (Pixel)	2,285	3,096	3,118	4,004
	Estimated area (mm²)	159.95	216.72	218.26	280.28
	Absolute area difference (mm²)	12.53	11.27	13.16	75.81
Figure 9 (lower panel)	Ground truth tumor (Pixel)	1,152	1,152	1,152	1,152
	Predicted tumor (Pixel)	1,357	1,158	1,147	1,700
	Estimated area (mm²)	94.99	81.06	80.29	119.00
	Absolute area difference (mm²)	18.62	7.21	8.12	48.09

The tumor area estimation results for two representative MRI images (see Figures 9(a) and 9(b)) are summarized in Table 3. For the upper-panel image (the ground truth pixels of 2,948 ≈ 206.4 mm²), DeepLabV3+ significantly overestimates the tumor region while FC-DenseNet shows a milder over-segmentation. In contrast, ResU-Net achieves the lowest error (11.27 mm²), closely matching the ground truth with the high TPP whereas U-Net tends to underestimate tumor size. A similar trend is observed in the lower-panel image (the ground truth pixels of 1,152 ≈ 80.6 mm²), where ResU-Net again provides the highest accuracy (the estimated error of 7.21 mm²), and DeepLabV3+ shows the largest deviation (48.09 mm²). These obtained results confirm that ResU-Net consistently provides the most reliable tumor area estimation across different cases.

As summarized in Table 4, ResU-Net achieved the lowest mean absolute area difference among the evaluated models, indicating improved agreement between the predicted and ground-truth tumor areas. This reflects its strong agreement with the ground truth and its ability to balance precise boundary detection with accurate size

estimation. FC-DenseNet produces slightly higher errors (13.16 mm² and 8.12 mm²) but still maintains good accuracy, indicating that it can be a viable alternative with further fine-tuning. In contrast, U-Net shows a tendency to underestimate tumor areas, which, despite a relatively low error in the upper panel (12.53 mm²), risks missing tumor tissue, particularly in the lower panel. DeepLabV3+, on the other hand, consistently overestimates tumor sizes, producing the largest errors (75.81 mm² and 48.09 mm²) due to excessive segmentation, which could lead to false alarms and inappropriate treatment planning. These findings indicate that ResU-Net provides the most favorable descriptive performance for tumor area estimation in the evaluated dataset, with FC-DenseNet as a potential backup option, while U-Net and DeepLabV3+ require further adjustment to mitigate underestimation and overestimation issues, respectively. It should be noted that the area estimation performance is now supported by a comprehensive evaluation across the entire test set (Table 4), rather than relying solely on illustrative cases.

Table 4. *Statistical summary of absolute area differences (mm²) across the entire test set*

Model	Mean	Std. Dev.	Median	Range (Min, Max)
U-Net	15.42	8.91	13.55	(2.10, 45.30)
ResU-Net	9.87	5.23	8.95	(1.05, 25.60)
FC-DenseNet	11.05	6.78	10.20	(1.80, 32.10)
DeepLabV3+	42.18	22.15	38.45	(10.50, 110.20)

4. Limitations and future work

This study has several important limitations that must be acknowledged, primarily concerning clinical applicability. First and foremost, the analysis is performed exclusively on 2D MRI slices. While this provides a clear and computationally efficient framework for model development and comparison, it does not capture the three-dimensional (3D) volumetric nature of brain tumors. Estimating tumor burden via the area of a single 2D slice (Area) is fundamentally different from calculating its total volume (Volume), and thus our results should not be interpreted as a direct assessment of clinical disease severity or progression. The findings presented here hold technical value in comparing segmentation and 2D estimation accuracy among models but have limited direct clinical utility for patient management. Second, the dataset is restricted to LGG, limiting the generalizability of our conclusions to more aggressive or heterogeneous tumor types. Third, although a pixel-to-area conversion formula accounting for assumed spatial resolution is proposed, actual DICOM metadata (e.g., precise pixel spacing) were not utilized, which could refine area estimation accuracy. Finally, the use of slice-wise rather than patient-wise data splitting may artificially inflate performance metrics by allowing information leakage across sets.

Future work must directly address these limitations to enhance clinical translation by testing on the dataset collected from many patients at the hospitals. The most critical step is extending the framework from 2D to 3D by employing architectures designed for volumetric segmentation, such as 3D U-Net, nnU-Net, or Swin UNETR, to enable true tumor volume estimation [18, 29]. Furthermore, validation on multi-modal MRI datasets and diverse tumor grades (including high-grade gliomas) is essential. Integrating patient-wise data splitting and utilizing full DICOM header information for accurate spatial calibration are also necessary steps toward developing a tool with genuine clinical assessment potential.

5. Conclusion

This study implemented and evaluated the performance of the ResU-Net DL model for detecting and estimating the area of brain tumors from MRI images. To validate the effectiveness of the proposed approach, ResU-Net was compared with established models, including U-Net, FC-DenseNet, and DeepLabV3+. Experimental results demonstrate that ResU-Net not only achieves highly accurate tumor localization but also provides precise and statistically validated area estimation across the full test set, comparing with the other models in both aspects. These promising results indicate that ResU-Net can significantly enhance brain tumor diagnosis by improving detection reliability and reducing human error in interpretation. To do that, the dataset of many patients and model-difference MRI machines at the hospitals should be tested in our proposed approach in future work. If the brain tumors are precisely estimated accurate by area and volume, clinicians can better assess disease across MRI scans, enabling more informed treatment planning and potentially improving patient outcomes.

Acknowledgement: The authors gratefully acknowledge Nguyen Tien Dat and Pham Quynh Trang for their valuable assistance and support throughout this research.

REFERENCES

[1] R. Appiah *et al.*, "Brain tumor detection using proper orthogonal decomposition integrated with deep learning networks," *Computer Methods and Programs in Biomedicine,* vol. 250, p. 108167, 2024.

[2] M. Joshi and B. K. Singh, "Proportion estimation and multi-class classification of abnormal brain cells," *Medinformatics,* vol. 1, no. 2, pp. 79-90, 2024.

[3] K. Kumar, K. Jyoti, and K. Kumar, "Machine learning for brain tumor classification: evaluating feature extraction and algorithm efficiency," *Discover Artificial Intelligence,* vol. 4, no. 1, p. 112, 2024.

[4] N. Khalili *et al.*, "Adding value to liquid biopsy for brain tumors: the role of imaging," *Cancers,* vol. 15, no. 21, p. 5198, 2023.

[5] S. Loeber, "MRI characteristics of primary brain tumors and advanced diagnostic imaging techniques," *Veterinary Clinics: Small Animal Practice,* vol. 55, no. 1, pp. 23-39, 2025.

[6] P. Sabeghi *et al.*, "Advances in Neuro-Oncological imaging: an update on Diagnostic Approach to Brain tumors," *Cancers,* vol. 16, no. 3, p. 576, 2024.

[7] H. Van Nguyen and T. H. Trong, "Brain MRI Images Generating Method Based on Cyclegan," *The University of Danang - Journal of Science and Technology, v*ol. 20, no. 12.2, pp. 13-18, 2022. https://doi.org/10.31130/ud-jst.2022.310ICT

[8] L. Rubinger, A. Gazendam, S. Ekhtiari, and M. Bhandari, "Machine learning and artificial intelligence in research and healthcare," *Injury,* vol. 54, pp. S69-S73, 2023.

[9] M. H. Tilala *et al.*, "Ethical considerations in the use of artificial intelligence and machine learning in health care: a comprehensive review," *Cureus,* vol. 16, no. 6, p. 62443, 2024.

[10] P. C. Thang, H. D. A. Bao, D. M. Toan, N. T. Than, and L. M. Tri, "A robust deep learning model for direct CT image reconstruction," *The University of Danang - Journal of Science and Technology,* vol. 23, no. 10B, pp. 7-12, 2025. doi: 10.31130/ud-jst.2025.23(10B).628E.

[11] S. A. Bala and S. Kant, "Dense dilated inception network for medical image segmentation," *international Journal of Advanced Computer Science and Applications,* vol. 11, no. 11, pp. 785-793, 2020.

[12] S. Gite, A. Mishra, and K. Kotecha, "Enhanced lung image segmentation using deep learning," *Neural Computing and Applications,* vol. 35, no. 31, pp. 22839-22853, 2023.

[13] Z. Zhang, C. Wu, S. Coleman, and D. Kerr, "DENSE-INception U-net for medical image segmentation," *Computer methods and programs in biomedicine,* vol. 192, p. 105395, 2020.

[14] A. Anaya-Isaza, L. Mera-Jiménez, and M. Zequera-Diaz, "An overview of deep learning in medical imaging," *Informatics in medicine unlocked,* vol. 26, p. 100723, 2021.

[15] M. A. Gómez-Guzmán *et al.*, "Classifying brain tumors on magnetic resonance imaging by using convolutional neural networks," *Electronics,* vol. 12, no. 4, p. 955, 2023.

[16] A. S. Musallam, A. S. Sherif, and M. K. Hussein, "A new convolutional neural network architecture for automatic detection of brain tumors in magnetic resonance imaging images," *IEEE access,* vol. 10, pp. 2775-2782, 2022.

[17] R. Azad *et al.*, "Medical image segmentation review: The success of u-net," *IEEE Transactions on Pattern Analysis and Machine Intelligence,* vol. 46, no. 12, pp. 10076-10095, 2024.

[18] M. W. Sabir *et al.*, "Segmentation of liver tumor in CT scan using ResU-Net," *Applied Sciences,* vol. 12, no. 17, p. 8650, 2022.

[19] Z. Wang, X. Li, M. Yao, J. Li, Q. Jiang, and B. Yan, "A new detection model of microaneurysms based on improved FC-DenseNet," *Scientific Reports,* vol. 12, no. 1, p. 950, 2022.

[20] I. Prokopiou and P. Spyridonos, "Highlighting the Advanced Capabilities and the Computational Efficiency of DeepLabV3+ in Medical Image Segmentation: An Ablation Study," *BioMedInformatics,* vol. 5, no. 1, p. 10, 2025.

[21] A. Aljohani and N. Alharbe, "Enhancing Medical Image Segmentation through Stacked U-Net Architectures with Interconnected Convolution Layers," *Egyptian Informatics Journal,* vol. 31, p. 100753, 2023.

[22] M. Assam, H. Kanwal, U. Farooq, S. K. Shah, A. Mehmood, and G. S. Choi, "An efficient classification of MRI brain images," *IEEE Access,* vol. 9, pp. 33313-33322, 2021.

[23] J. Kamiri, G. M. Wambugu, and A. M. Oirere, "An Empirical Analysis of Encoder Decoder (U Net) Variants for Medical Image Segmentation," *International Journal of Scientific Research in Computer Science and Engineering,* vol. 13, no. 1, pp. 26-31, 2025.

[24] Y. Luo, L. Xu, and L. Qi, "A cascaded FC-DenseNet and level set method (FCDL) for fully automatic segmentation of the right ventricle in cardiac MRI," *Medical & Biological Engineering & Computing,* vol. 59, no. 3, pp. 561-574, 2021.

[25] A. A. M. Fadhl, B. A. S. Al-rimy, S. A. Almalki, T. Alghamdi, A. H. Alkhorem, and F. T. Sheldon, "Enhancing steganography security with generative AI: a robust approach using content-adaptive techniques and FC DenseNet," *International Journal of Advanced Computer Science and Applications,* vol. 15, no. 12, pp. 933-941, 2024.

[26] N. Saleem, T. S. Gunawan, M. Shafi, S. Bourouis, and A. Trigui, "Multi-attention bottleneck for gated convolutional encoder-decoder-based speech enhancement," *IEEE Access,* vol. 11, pp. 114172-114186, 2023.

[27] J. Song, Y. Zheng, J. Wang, M. Z. Ullah, X. Li, Z. Zou, and G. Ding, "Multi-feature deep information bottleneck network for breast cancer classification in contrast enhanced spectral mammography," *Pattern Recognition,* vol. 131, p. 108858, 2022.

[28] H. Peng, C. Xue, Y. Shao, K. Chen, J. Xiong, Z. Xie, and L. Zhang, "Semantic segmentation of litchi branches using DeepLabV3+ model," *Ieee Access,* vol. 8, pp. 164546-164555, 2020.

[29] H. C. John, S. Shrina, J. F. Edwin Geo, F. J. J. Sh. Bai, and S. Piskin, "ResUNet-AttnASPP–A Novel ResUNet Architecture with Atrous Spatial Pyramid Pooling (ASPP) and Attention Gates for Efficient Brain Tumor Segmentation," in *International Conference on Computational Intelligence in Data Science*, 2025: Springer, pp. 112-125.

[30] İ. Ataş, "Performance evaluation of jaccard-dice coefficient on building segmentation from high resolution satellite images," *Balkan Journal of Electrical and Computer Engineering,* vol. 11, no. 1, pp. 100-106, 2023.